

Josephson radiation patterns in underdamped topological Josephson junctions

Yuejian Zhang,¹ Xiping Yang,¹ Jia-Jin Feng,² Zhi Wang,^{2,*} and Tianxing Ma^{1,3,†}

¹Department of Physics, Beijing Normal University, Beijing 100875, China

²School of Physics, Sun Yat-sen University, Guangzhou 510275, China

³Beijing Computational Science Research Center, Beijing 100193, China

(Dated: March 26, 2025)

Majorana zero mode is a unique quasiparticle state on the edge of topological superconductors. For Josephson junctions with Majorana zero modes, there will be 4π -periodic current components in the current-phase relation. Within the quantum resistively and capacitively shunted junction model, we study the dynamics of the Josephson phase which is correlated with the Majorana two-level system through the 4π -periodic Josephson effect, and show that the feedback of the quantum oscillation of the Majorana two-level system induces an oscillatory pattern in the Josephson radiation spectra. We numerically study this radiation spectra and find that the unique oscillatory patterns universally exist in the underdamped junction regime. We solve the model analytically for typical junction parameters and find solutions of the Bessel function form which explains the main features of the oscillation patterns in the Josephson radiation.

I. INTRODUCTION

In recent development of quantum computation¹, a fault-tolerant scheme has been theoretically proposed based on the premises of non-Abelian statistics of quasiparticles. Such bizarre statistic can appear in superconducting systems for the so-called Majorana zero modes^{2,3}, which can construct noise resistant topological qubits. Braiding Majorana zero modes around one another execute quantum gate operations whose precession is protected by the topology of the braiding paths. Majorana zero modes are theoretically introduced in p -wave superconductors and experimentally engineered by putting an s -wave superconductor in proximity to a semiconductor with appropriate spin-orbit coupling and Zeeman field^{2,4,5}. Differential conductance are widely used as signatures of Majorana zero mode⁶. In addition, many recent experiments are focusing on transport and spectroscopic properties of Josephson junctions between two topological superconductors^{2,7–11}.

In topological junctions, Majorana zero modes carry a supercurrent which is 4π -periodic in Josephson phase, known as the fractional Josephson effect^{5,12,13}. Hybridization of Majorana zero modes break the exact 4π periodicity, making the direct transport measurement of 4π periodicity difficult. Recent experimental efforts are concentrated on studying dynamical properties such as electromagnetic radiation from the junction^{14–16}. This Josephson radiation was predicted by standard resistively shunted junction model to have a series of spectra with frequencies $f = neV/h$ ^{17,18}, where the first one $f_M = eV/h$ corresponds to the 4π -period Josephson effect and the second one $f_J = 2eV/h$ corresponds to conventional 2π -period Josephson effect^{12,19–21}. Several recent experiments successfully observed the 4π -period Josephson radiation with frequency f_M , but its relation to the Majorana zero modes are still under debate because the signals lacks smoking gun features to be

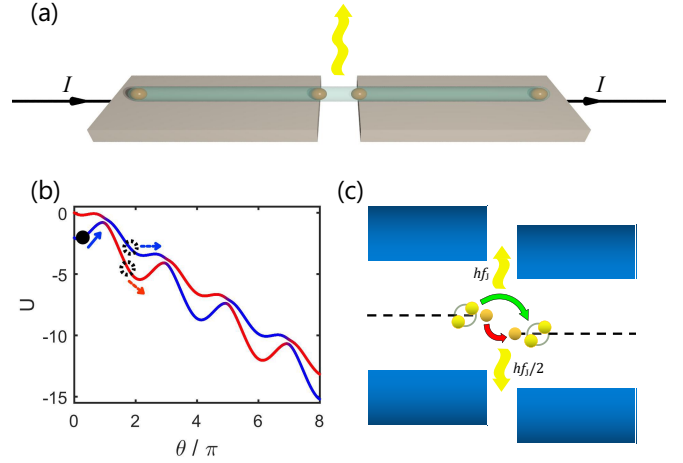


FIG. 1. (a) Setup for a Josephson junction with Majorana zero modes. Upon current injection above the critical current, the voltage across the junction oscillates and radiates electro-magnetic waves. (b) The washboard picture for the quantum resistively shunted junction model. The junction is equivalenced with the classical motion of a particle with a quantum spin. (c) The semiconductors picture for the Josephson radiation. The coherent Cooper pair tunneling result in a radiation with frequency $f_J = 2eV/h$, while the coherent single particle tunneling through the Majorana zero modes contribute a radiation with frequency $f_M = eV/h$.

determined uniquely from Majorana zero modes^{12,20,22}.

Hybridization of Majorana zero modes leads to a quantum two-level system⁶, with its Hamiltonian determined by the Josephson phase. We have included this Majorana two-level system into the standard theory, and built a quantum resistively and capacitively shunted junction model to study the dynamics of the topological Josephson junction^{10,18,23–25}. Inspired by recent experiments, we perform frequency analysis within this model and calculate the Josephson radiation. The

setup for a Josephson junction with Majorana zero modes has shown in Fig.1(a). We concentrate our study on the underdamped junctions which was shown to demonstrate richer dynamical behaviors due to the shunted capacitance²³. We numerically reveal an unique oscillatory pattern in the spectra, which is due to the quantum oscillation of the Majorana two-level system. For a typical limiting parameter, we analytically solve the equations and find a solution of Bessel function which satisfactorily captures the main structures of the oscillation patterns. Our work provides one additional signature for Majorana zero modes²².

II. QUANTUM RESISTIVELY AND CAPACITIVELY SHUNTED JUNCTION MODEL.

The quantum resistively shunted junction model was introduced in Ref.^{26,27}. Within this framework, the dynamics of the Josephson junction is reduced to a set of nonlinear equations²⁶, which can be interpreted as equations of motion for a classical particle with spin one-half, subjecting a one dimensional spin-dependent potential energy as shown in Fig.1(b). This model contains the least ingredients to describe the dynamics of the Josephson phase and the wave function of the Majorana two-level system²³. The equations of motion are given by,

$$\frac{\hbar C \ddot{\theta}}{2eI} + \frac{\hbar \dot{\theta}}{2eRI} = 1 - I_1 \sin \theta - I_2 \langle i\gamma_L \gamma_R \rangle \sin \frac{\theta}{2}, \quad (1)$$

where R is the resistance of the junction and C is the capacitance, θ is the Josephson phase, I is the injected dc current, $I_1 = I_{c1}/I$ with I_{c1} the Josephson current from the trivial part of superconductor^{2,5,28-32}, $I_2 = I_{c2}/I$ with I_{c2} the topological Josephson current contributed by Majorana zero modes, and $\psi_{0,1}$ are the two components of the wave function for the two-level system². In this model, the quantum dynamics of the two-level system is included by the Schrödinger equation which couples θ and ψ ^{24,33,34},

$$i\hbar \frac{d}{dt} \begin{pmatrix} \psi_0 \\ \psi_1 \end{pmatrix} = \begin{pmatrix} E_M \cos \frac{\theta}{2} & \delta \\ \delta & -E_M \cos \frac{\theta}{2} \end{pmatrix} \begin{pmatrix} \psi_0 \\ \psi_1 \end{pmatrix}, \quad (2)$$

where E_M is the Josephson energy from the coupling of the Majorana zero modes in the junction, and δ is the hybridization energy from the wave function overlapping of the distant Majorana zero modes in the same side of the junction.

III. UNDERDAMPED JUNCTION AND OSCILLATING EMISSION PATTERN

Upon injection of a current above the critical value, the Josephson phase begins to increase with an oscillating speed³², whose motion correlates with the quantum dynamics of the two-level system. Since the speed

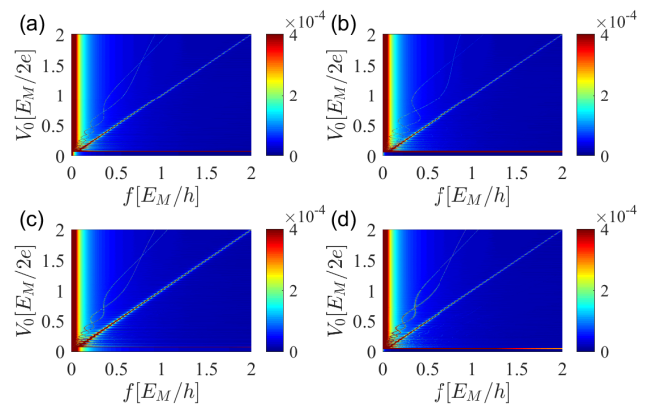


FIG. 2. Radiation frequency spectrum for underdamped junction simulated with QRCSJ model. Parameters used are:(a) $E_M = 78.4\mu\text{eV}$, $I_{c1} = 63\text{nA}$, $I_{c2} = 8\text{nA}$, $C = 0.1\text{nF}$, $R = 50\Omega$, $\delta/E_M = 0.1$, $I \in [0, 2]\mu\text{A}$ in Eqs.(1) and (2); (b) $\delta/E_M = 0.2$; (c) $C = 0.05\text{nF}$; (d) $I_M = 32\text{nA}$. The other parameters of (b)-(d) are same as (a).

of the Josephson phase gives the voltage according to the second Josephson relation $V = \hbar\dot{\theta}/2e$, an oscillating speed of Josephson phase means an oscillating voltage, which, combining with injected dc current, gives an electromagnetic radiation, the so-called Josephson radiation. In order to obtain the radiation spectrum from the quantum resistively shunted junction mode, we first simulate the dynamics of the phase difference and obtain the time evolution of the voltage $V(t)$ ^{24,33,34}. From this time dependent function, we can obtain the dc voltage by integration $V_0 = \int dt V(t)$, and obtain the spectrum function through Fourier transformation, $V(f) = \int dt e^{i2\pi ft} V(t)$ ²⁷. Since a dc current is injected, this ac voltage spectrum is exactly the radiation spectrum from the quantum resistively shunted junction model¹⁸.

We simulate the coupled equations Eq. (1) and (2), and calculated the time evolution of the voltage. We demonstrate the radiation spectra for typical junction parameters in Fig.2. It is clear that besides from the AC Josephson radiation line, whose position is $f = \frac{2e}{h}V_0$, there are also two oscillating radiation lines caused by MZMs, which are symmetric with respect to $f = \frac{e}{h}V_0$. The oscillation radiation shows the unique properties of MZM in underdamped Josephson junction.

IV. ANALYTICALLY SOLUTIONS FOR LANDAU-ZENER-STÜCKELBERG INTERFERENCE

Here we analytically study the underdamped regime for the Josephson junction¹¹. When the injected current of the Josephson junction is beyond the critical current of the junction^{32,35}, a voltage drop appears and the

superconducting phase difference starts to evolve with time according to the renowned AC Josephson relation. In the present system this triggers a quantum mechanical evolution of the MZMs. When the system is driven dynamically accrossing $\theta = (2n + 1)\pi$, the quantum state of the Majorana TLS may either stay in its original parity state³³, or evolve into the opposite parity state. The probability for staying in the same state is given by the ratio between the crossing-avoid energy and the velocity of the phase variation $\propto \exp[-\delta^2/(\hbar\omega E_M)]$ with $\omega = d\theta/dt$, as was first revealed by Landau and Zener. Experiencing many passages through the $\theta = (2n + 1)\pi$, the occupation probabilities of the two parity states are governed by the accumulation of quantum phases acquired at individual passages known as the LZS interference, which yields a second, longer time scale as compared with the period of the oscillation of superconducting phase difference².

For an applied DC current³², the voltage has a dominant DC voltage part V_0 which determines the dynamics of the Josephson phase^{24,33,34}. For the lowest order approximation, we assume that the Josephson phase is purely driven by this DC voltage.

We have $\theta \approx \omega_J t$ ($\omega_J = 2\pi f_J$) which could be substituted into the Schrödinger equation (2) to decouple it from the RCSJ equation (1). After this simplification the Hamiltonian is time periodic. It can be tackled in terms of the Floquet theory, which can be taken as the time version of the Bloch theorem. In general, the solution can be given in the form

$$\Psi(t) \equiv (\psi_0, \psi_1)^T = \tilde{\psi}(t)e^{-iQt}, \quad (3)$$

with $\tilde{\psi}(t)$ a time periodic function with the same period as the Hamiltonian $\tilde{\psi}(t) = \tilde{\psi}(t + 4\pi/\omega_J)$, and Q the eigenvalue to be determined. It is natural to decompose the Hamiltonian, and accordingly the wave function, into Fourier components

$$\mathcal{H} = \sum_n \mathcal{H}_n e^{in\omega_J t/2}, \quad \tilde{\psi}(t) = \sum_n \tilde{\psi}_n e^{in\omega_J t/2}, \quad (4)$$

with the Hamiltonian components

$$\mathcal{H}_0 = \begin{pmatrix} 0 & \delta \\ \delta & 0 \end{pmatrix}, \quad \mathcal{H}_{\pm 1} = \begin{pmatrix} E_M/2 & 0 \\ 0 & -E_M/2 \end{pmatrix}, \quad (5)$$

and all other matrices are zero in the present case. Plugging them back into Eq. (2), we arrive at the following static secular equation,

$$\sum_l \left(\mathcal{H}_{n-l} + \frac{n\omega_J}{2} \delta_{nl} \hat{I} \right) \tilde{\psi}_l = Q \tilde{\psi}_n, \quad (6)$$

with \hat{I} the 2x2 identity matrix. Defining a vector $\tilde{\Psi} = (\dots, \tilde{\psi}_{-1}, \tilde{\psi}_0, \tilde{\psi}_1, \dots)^T$, we obtain the time-independent Floquet Hamiltonian

$$\mathcal{H}_f = \begin{pmatrix} \mathcal{H}_0 - \omega_J \hat{I} & \mathcal{H}_1 & 0 & 0 & 0 & \dots \\ \mathcal{H}_1 & \mathcal{H}_0 - \frac{\omega_J}{2} \hat{I} & \mathcal{H}_1 & 0 & 0 & \dots \\ 0 & \mathcal{H}_1 & \mathcal{H}_0 & \mathcal{H}_1 & 0 & \dots \\ 0 & 0 & \mathcal{H}_1 & \mathcal{H}_0 + \frac{\omega_J}{2} \hat{I} & \mathcal{H}_1 & \dots \\ 0 & 0 & 0 & \mathcal{H}_1 & \mathcal{H}_0 + \omega_J \hat{I} & \dots \\ \dots & \dots & \dots & \dots & \dots & \dots \end{pmatrix} \quad (7)$$

Now the original system of two states with time-periodic Hamiltonian \mathcal{H} in Eq. (2) is transformed into a system with static Floquet Hamiltonian \mathcal{H}_f . The diagonal part of the Floquet Hamiltonian is built by infinite 2x2 blocks, with each block formed by the time-invariant part of the original Hamiltonian \mathcal{H}_0 adding energy quanta $n\omega_J/2$ associated with integer number of ‘‘photons’’; any two diagonal blocks with one-photon difference are connected by an off-diagonal 2x2 block given by the amplitude of time-periodic part in the original Hamiltonian. The basis states for the Floquet Hamiltonian \mathcal{H}_f are the Floquet states $|n, \alpha\rangle$, with α referring to the two states $|S_j\rangle$ ($j = 0$ and 1) and n to the Fourier component (or equivalently the number of photons). This Floquet Hamiltonian is static, and thus can be used to describe the quantum dynamics of the original 2x2 time-periodic Hamiltonian^{24,33}. Especially the transition probability between two quantum states $|\psi_0\rangle$ and $|\psi_1\rangle$ can be expressed as a summation of those between corresponding Floquet states $|0, \psi_0\rangle$ and $|n, \psi_1\rangle$

$$T_{|\psi_0\rangle \rightarrow |\psi_1\rangle} = \sum_n \left| \langle n, \psi_1 | e^{-i\mathcal{H}_f(t-t_0)} | 0, \psi_0 \rangle \right|^2. \quad (8)$$

Therefore, the problem of evaluating the transition probability between two quantum states governed by a time-dependent Hamiltonian is reduced to a task to solve a time-independent Floquet Hamiltonian, which can be treated by conventional techniques in quantum mechanics.

In the case with $\delta \ll \hbar\omega_J, E_M$ is under concern. We can divide the Floquet Hamiltonian into two parts

$$\mathcal{H}_f = H_0 + H', \quad (9)$$

with the perturbation term

$$H' = \delta \sum_n (|n, \psi_0\rangle \langle n, \psi_1| + |n, \psi_1\rangle \langle n, \psi_0|) \quad (10)$$

and H_0 is the rest of \mathcal{H}_f . It is noticed that, for $\delta = 0$, the solution of Eq. (2) can be given directly

$$\begin{aligned} \psi_0(t) &= e^{-2i \frac{E_M}{\hbar\omega_J} \sin \frac{\omega_J t}{2}} \psi_0(0), \\ \psi_1(t) &= e^{2i \frac{E_M}{\hbar\omega_J} \sin \frac{\omega_J t}{2}} \psi_1(0). \end{aligned} \quad (11)$$

Using the Jacobi-Anger expansion

$$e^{iz \sin \gamma} = \sum_{n=-\infty}^{+\infty} J_n(z) e^{in\gamma}, \quad (12)$$

where for the present case $z = -2E_M/(\hbar\omega_J)$ and $\gamma = \omega_J t/2$, the above solution can be decomposed into Fourier components

$$\begin{pmatrix} \psi_0(t) \\ \psi_1(t) \end{pmatrix} = \sum_{n=-\infty}^{\infty} \begin{pmatrix} J_n(z)\psi_0(0) \\ J_n(-z)\psi_1(0) \end{pmatrix} e^{in\gamma}, \quad (13)$$

with the form useful for Floquet analysis. With $\psi_0(0) = 0, \psi_1(0) = 1$ and $\psi_0(0) = 1, \psi_1(0) = 0$, we obtain two sets of Floquet eigenfunctions

$$\begin{aligned} \tilde{\Psi}_{+,0} &= (\dots, J_{-1}(z), 0, J_0(z), 0, J_1(z), 0, \dots)^T, \\ \tilde{\Psi}_{-,0} &= (\dots, 0, J_{-1}(-z), 0, J_0(-z), 0, J_1(-z), \dots)^T, \end{aligned} \quad (14)$$

associated with $Q_0 = 0$ where the subscript refers to the non-perturbed case. Due to the translational symmetry of the Floquet Hamiltonian, eigenfunctions associated with eigenvalues $Q_0 = n\omega_J/2$ are given straightforwardly as

$$\begin{aligned} \tilde{\Psi}_{+,n} &= (\dots, J_{n-1}(z), 0, J_n(z), 0, J_{n+1}(z), 0, \dots)^T, \\ \tilde{\Psi}_{-,n} &= (\dots, 0, J_{n-1}(-z), 0, J_n(-z), 0, J_{n+1}(-z), \dots)^T. \end{aligned} \quad (15)$$

Using these eigenfunctions as the new basis, one has the kinetic equivalent Hamiltonian $K_{0,m,n} = \tilde{I}\delta_{mn}n\omega_J/2$ and

$$\begin{aligned} K'_{n,m} &= \begin{pmatrix} \langle \tilde{\Psi}_{+,n} | H' | \tilde{\Psi}_{+,m} \rangle & \langle \tilde{\Psi}_{+,n} | H' | \tilde{\Psi}_{-,m} \rangle \\ \langle \tilde{\Psi}_{-,n} | H' | \tilde{\Psi}_{+,m} \rangle & \langle \tilde{\Psi}_{-,n} | H' | \tilde{\Psi}_{-,m} \rangle \end{pmatrix} \\ &= \delta \begin{pmatrix} 0 & \sum_i J_{i-n}(z) J_{i-m}(-z) \\ \sum_i J_{i-n}(-z) J_{i-m}(z) & 0 \end{pmatrix}. \end{aligned} \quad (16)$$

Exploiting the relations for Bessel functions

$$\sum_i J_{i-n}(z) J_{i-m}(-z) = J_{n-m}(2z), \quad (17)$$

we arrive at the kinetic perturbation Hamiltonian

$$K'_{n,m} = \delta \begin{pmatrix} 0 & J_{m-n}(2z) \\ J_{n-m}(2z) & 0 \end{pmatrix}. \quad (18)$$

Now the unperturbed part of Hamiltonian is diagonalized, while, as the price, the interaction part becomes complicated with more non-zero elements as compared that in Eq. (10). However, for the case $\delta \ll \hbar\omega_J, E_M$, only the transitions between $|0, \psi_0\rangle$ and $|0, \psi_1\rangle$ is important in Eq.(8) to the lowest-order perturbation, which results in the following 2x2 Floquet Hamiltonian

$$H_F = \begin{pmatrix} 0 & \delta J_0(2z) \\ \delta J_0(2z) & 0 \end{pmatrix}. \quad (19)$$

The evolution operator for this effective Floquet Hamiltonian is

$$\hat{U}(t) = e^{-i\hat{H}_F t/\hbar} = e^{-i\delta J_0(2z)\tau_x t/\hbar}, \quad (20)$$

which yields a quantum mechanical oscillation

$$|\psi_1(t)|^2 = \cos^2(\omega_{LZS}t), \quad |\psi_0(t)|^2 = \sin^2(\omega_{LZS}t) \quad (21)$$

and the polarization of the pseudo-spin formed by MZMs is

$$s = |\psi_1(t)|^2 - |\psi_0(t)|^2 = \cos(\omega_M t), \quad (22)$$

with the oscillation angular frequency

$$\omega_M = 2\omega_{LZS} = \frac{2\delta}{\hbar} J_0(2z) = \frac{2\delta}{\hbar} J_0\left(\frac{2E_M}{eV_0}\right). \quad (23)$$

starting from an initial state $\psi_0 = 0$ and $\psi_1 = 1$. This is the LZS interference of Majorana qubit states. The frequency of Majorana qubit rotation is linearly proportional to the interaction between the two parity states as can be understood intuitively. In contrary, the frequency ω associated with the increase of superconducting phase difference is involved in a nonlinear way^{2,26}, and does not influence much the Majorana qubit rotation for large frequency since the reduced probability for parity flipping at a single passage is compensated by the increasing number of passages.

V. JOSEPHSON RADIATION AND BESSEL SOLUTIONS

The LZS of the TLS wave function will influences the Josephson radiation of Eq. (1). We input a fixed DC current I and treat \tilde{V} as the perturbation of V_0 . To calculate the radiation, we only need the spectrum function of the voltage V . For this purpose, we expands V with the Fourier transformation

$$V(t) = \int_{-\infty}^{+\infty} v(\omega) e^{i\omega t} d\omega. \quad (24)$$

where $v(\omega)$ is the amplitude in frequency domain ω . The pure real function $V(t)$ requires that $v(-\omega) = v^*(\omega)$.

As the RCSJ equation involves periodic functions, we can safely assume that V have discrete spectrum and write down the expansion in the form of,

$$v(\omega) = V_0\delta(\omega) + \frac{1}{2} \sum_n [V_n\delta(\omega - \omega_n) + V_n^*\delta(\omega + \omega_n)], \quad (25)$$

where $\omega_n > 0$ represents the peaks in the radiation spectrum. The factor 1/2 makes $|V_n|$ directly the measure strength of angular frequency ω_n and $\arg(V_n)$ is the phase which also be convenient for later calculation. With this simplified expansion, we can explicitly express the inverse Fourier transformation in the pure real form that

$$\begin{aligned} V(t) &= V_0 + \frac{1}{2} \sum_n [V_n e^{i\omega_n t} + V_n^* e^{-i\omega_n t}] \\ &= V_0 + \sum_n [a_n \cos(\omega_n t) + b_n \sin(\omega_n t)], \end{aligned} \quad (26)$$

where we define $a_n \equiv (V_n + V_n^*)/2$, $b_n \equiv i(V_n - V_n^*)/2$.

Now we explore the expression for the Josephson phase θ since that is the variable for the RCSJ equation. The integration of the second Josephson relation $d\theta/dt = 2eV/\hbar$ using Eq. (26) gives

$$\theta = \theta_0 + \frac{2e}{\hbar} V_0 t + \frac{2e}{\hbar} \sum_n \left(\frac{a_n}{\omega_n} \sin \omega_n t - \frac{b_n}{\omega_n} \cos \omega_n t \right) \quad (27)$$

where the constant θ_0 is decided by the initial condition. For convenience, we will use $\omega_J = \frac{2e}{\hbar} V_0$ to simplify the factor.

Now we put the expression for θ back into the sine functions of Eq.(1), and try to obtain an explicit expansion. For this purpose, a mathematically convenient method is to write the sine functions in the exponential form,

$$\sin \theta = \frac{i}{2} (e^{-i\theta} - e^{i\theta}). \quad (28)$$

Then we try to expand the exponential functions with Bessel functions. For the first term, we substitute Eq. (27) in it and obtain

$$e^{i\theta} = e^{i(\omega_J t + \theta_0)} \prod_n e^{i \frac{2ea_n}{\hbar\omega_n} \sin \omega_n t} e^{-i \frac{2eb_n}{\hbar\omega_n} \cos \omega_n t}. \quad (29)$$

We define $A_n \equiv 2ea_n/(\hbar\omega_n)$ and $B_n \equiv 2eb_n/(\hbar\omega_n)$. They also can be expressed using V_n

$$A_n = \frac{e}{\hbar\omega_n} (V_n + V_n^*) \quad B_n = \frac{e}{\hbar\omega_n} (V_n - V_n^*) \quad (30)$$

Using Jacobi-Anger expansion $e^{iz \sin x} = \sum_{n=-\infty}^{+\infty} J_n(z) e^{inx}$ and $e^{iz \cos x} = \sum_{n=-\infty}^{+\infty} i^n J_n(z) e^{inx}$, we arrive at

$$e^{i\theta} = e^{i(\omega_J t + \theta_0)} \prod_n \sum_{p,q=-\infty}^{\infty} i^q J_p(A_n) J_q(-B_n) e^{i(p+q)\omega_n t} \quad (31)$$

Up to now, all the formulas are exact. In order to obtain analytical solutions, now we begin to make approximations. Using the fact that $J_0 \gg J_1 \gg \dots$, we can discard most of terms in this polymerization of Eq. (31). We keep the zero order term just contained J_0 and the first order term just contained one $J_{\pm 1}$ with all other factors purely J_0 . Then the formula is simplified to,

$$e^{i\theta} \approx e^{i(\omega_J t + \theta_0)} \left[j_0 + \sum_n (j_n e^{i\omega_n t} - j_n^* e^{-i\omega_n t}) \right], \quad (32)$$

for simplicity we define,

$$j_0 = \prod_n J_0(A_n) J_0(B_n) \\ j_n = j_0 \frac{J_1(A_n) J_0(B_n) - i J_0(A_n) J_1(B_n)}{J_0(A_n) J_0(B_n)}. \quad (33)$$

Here we have use the relation $J_{-1}(x) = J_1(-x) = -J_1(x)$ and $J_0(-x) = J_0(x)$. We return it to the sine function

and get

$$\sin \theta \approx -\frac{i}{2} e^{i(\omega_J t + \theta_0)} \left[j_0 + \sum_n (j_n e^{i\omega_n t} - j_n^* e^{-i\omega_n t}) \right] + \text{h.c.} \quad (34)$$

In the same way, we can expand the $\sin \theta/2$ term, and obtain the expression up to the first-order of J_1 as,

$$\sin \frac{\theta}{2} \approx -\frac{i}{2} e^{i(\frac{\omega_J}{2} t + \frac{\theta_0}{2})} \left[l_0 + \sum_n (l_n e^{i\omega_n t} - l_n^* e^{-i\omega_n t}) \right] + \text{h.c.} \quad (35)$$

where for simplicity we define

$$l_0 = \prod_n J_0\left(\frac{A_n}{2}\right) J_0\left(\frac{B_n}{2}\right) \\ l_n = l_0 \frac{J_1\left(\frac{A_n}{2}\right) J_0\left(\frac{B_n}{2}\right) - i J_0\left(\frac{A_n}{2}\right) J_1\left(\frac{B_n}{2}\right)}{J_0\left(\frac{A_n}{2}\right) J_0\left(\frac{B_n}{2}\right)} \quad (36)$$

Now we look at the other terms in Eq. (1). The time derivative of the voltage is written as

$$\frac{dV}{dt} = \frac{1}{2} \sum_n (i\omega_n V_n e^{i\omega_n t} - i\omega_n V_n^* e^{-i\omega_n t}). \quad (37)$$

The time evolution of the TLS is assumed to be already known, with an oscillation function obtained in the last section,

$$s \approx s_1 e^{i\omega_M t} + s_1^* e^{-i\omega_M t}, \quad (38)$$

where s_1 is constant and the ω_M have been obtained in Eq. (23). Replaced by Eq. (26), Eq. (37), Eq. (34), Eq. (35) and Eq. (38), the fully expansion of Eq. (1) can be written as

$$2 \left(\frac{V_0}{R} - I \right) + \sum_n \left(\frac{1}{R} + i\omega_n C \right) V_n e^{i\omega_n t} \\ = iI_{c1} j_0 e^{i(\omega_J t + \theta_0)} \\ + iI_{c2} l_0 s_1 e^{i\left[\left(\frac{\omega_J}{2} + \omega_M\right)t + \frac{\theta_0}{2}\right]} + iI_{c2} l_0 s_1^* e^{i\left[\left(\frac{\omega_J}{2} - \omega_M\right)t + \frac{\theta_0}{2}\right]} \\ + \sum_n \left\{ iI_{c1} j_n e^{i[(\omega_J + \omega_n)t + \theta_0]} - iI_{c1} j_n^* e^{i[(\omega_J - \omega_n)t + \theta_0]} \right. \\ + iI_{c2} s_1 l_n e^{i\left[\left(\frac{\omega_J}{2} + \omega_M + \omega_n\right)t + \frac{\theta_0}{2}\right]} - iI_{c2} s_1 l_n^* e^{i\left[\left(\frac{\omega_J}{2} + \omega_M - \omega_n\right)t + \frac{\theta_0}{2}\right]} \\ \left. + iI_{c2} s_1^* l_n e^{i\left[\left(\frac{\omega_J}{2} - \omega_M + \omega_n\right)t + \frac{\theta_0}{2}\right]} - iI_{c2} s_1^* l_n^* e^{i\left[\left(\frac{\omega_J}{2} - \omega_M - \omega_n\right)t + \frac{\theta_0}{2}\right]} \right\} \\ + \text{h.c.} \quad (39)$$

where we have multiplied the equation by 2 and rearrange V_0 and V_n to the LHS. Using the fact that two Fourier eigenfunctions are orthogonal,

$$\frac{1}{2\pi} \int_{-\infty}^{+\infty} e^{-i\omega_m t} V_n e^{i\omega_n t} dt = V_n \delta(\omega_m - \omega_n), \quad (40)$$

we can calculate V_n by multiplying both sides of Eq. (39) with $e^{-i\omega_n t}$ and then integrate over the full time range. We find that $V_n \neq 0$ only for the discrete frequencies of

$$\omega_n = p \frac{\omega_J}{2} + q \omega_M \quad (p, q, \frac{p+q}{2} \in Z, \omega_n > 0), \quad (41)$$

where the lowest order radiation frequencies are explicitly written as,

$$\omega_1 = \frac{\omega_J}{2} - \omega_M, \quad \omega_2 = \frac{\omega_J}{2} + \omega_M, \quad \omega_3 = \omega_J. \quad (42)$$

Recalling Eq. (23), this give the radiation spectra of

$$f_1 = \frac{f_J}{2} - \frac{\delta}{\hbar\pi} J_0 \left(\frac{2E_M}{eV_0} \right), \quad (43)$$

$$f_2 = \frac{f_J}{2} + \frac{\delta}{\hbar\pi} J_0 \left(\frac{2E_M}{eV_0} \right) \quad (44)$$

$$f_3 = f_J. \quad (45)$$

These three functions are plotted in Fig. 3(b) which is quite similar to the numerical results of Fig.3(a) for high DC voltage regimes. It proves that our argument holds up.

As shown in Eqs.(43) and (44), the oscillation amplitude of radiation lines caused by MZM depends on δ . In the case of large δ , the oscillation amplitude is large and oscillatory pattern almost overlaps with each other. Novel radiation characteristics will appear in the radiation pattern, such as Fig.4(a), where the oscillation lines of different orders are connected with each other to form a radiation spectrum with negative slopes. We show the analytic explanation of this phenomenon in Fig.4(b), where the red lines are the radiation lines caused by AC Josephson current $f_J^n = n f_J = \frac{2neV_0}{h}$, $n = 1, 2, 3, \dots$, and the blue dotted lines are radiation caused by MZMs approximately described by Bessel function $f_M^n = \frac{(2n-1)eV_0}{h} \pm \frac{2\delta}{h} J_0 \left(\frac{2E_M}{eV_0} \right)$, $n = 1, 2, 3, \dots$

The intersections of two f_M^n rays of the same order n are zero points of $J_0 \left(\frac{2E_M}{eV_0} \right)$. If these points are connected with each other in the way shown by the black solid line in Fig.4(b), we can find that the connected black line overlaps with the radiation line caused by MZMs. That's why there seems to be new radiation lines when δ is large. Mathematically, Bessel function is approximated as trigonometric function, and we can figure out the analytic expression of black solid lines,

$$\frac{f}{(E_M/h)} = -(l - \frac{3}{4}) \frac{V}{E_M/2e} + \frac{4}{\pi}, \quad (46)$$

where l can be any integer. The analytical results show that the novel radiations have a common cross section $\frac{4}{\pi}$ as shown in Fig.4(b). There is a certain difference between the numerical and analytical results, because the perturbation calculation is quite different from the real condition when δ is large.

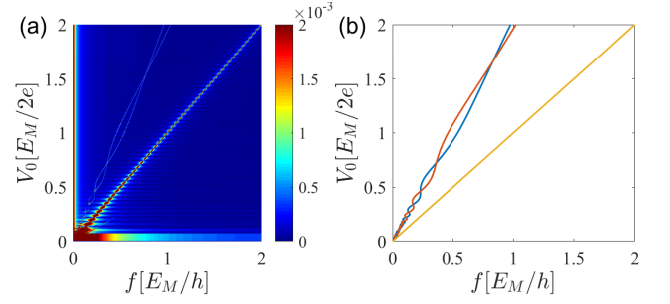


FIG. 3. (a) Radiation frequency spectrum for typical underdamped junctions simulated with QRCSJ model. The parameter is same as Fig.2 except $C = 10^3 * 2e^3 / (\hbar I_{c2})$ and $\delta = 0.05 E_M$. (b) The lowest order oscillation frequency of the analytical results.

VI. RADIATION POWER

Finally we examine the radiation intensity for these lowest order radiation frequencies and take the approximation that the contribution from ω_1 , ω_2 and ω_3 dominant the summation in Eq.(39). Then for these three frequencies, we obtain three equations respectively

$$\begin{aligned} \left(\frac{1}{R} + i\omega_1 C \right) V_1 &= iI_{c2} l_0 s_1^* e^{i\frac{\theta_0}{2}} - iI_{c1} j_2^* e^{i\theta_0} \\ \left(\frac{1}{R} + i\omega_2 C \right) V_2 &= iI_{c2} l_0 s_1 e^{i\frac{\theta_0}{2}} - iI_{c1} j_1^* e^{i\theta_0} \\ \left(\frac{1}{R} + i\omega_3 C \right) V_3 &= iI_{c1} j_0 e^{i\theta_0} + iI_{c2} s_1 l_1 e^{i\frac{\theta_0}{2}} + iI_{c2} s_1^* l_2 e^{i\frac{\theta_0}{2}} \end{aligned} \quad (47)$$

where the functions $j_{0,1}$ and $l_{0,1,2}$ are functions of $A_{1,2,3}$ and $B_{1,2,3}$ as defined in Eqs. (33) and (36), with the parameters A_n , B_n in Eq. (30). In the regime of our study where $I \gg I_{c1} + I_{c2}$, we should have $A_n, B_n \ll 1$. As zero's order approximation we only take $J_0 \approx 1$ and neglect all higher order Bessel functions in Eqs. (33) and (36). We obtain

$$j_0 = l_0 = 1, \quad j_n = l_n = 0. \quad (48)$$

Plugging this expression back into the equation, we obtain The solution for V_n as,

$$V_1 = \frac{I_{c2} s_1^* e^{i(\frac{\theta_0}{2} + \frac{\pi}{2})}}{\frac{1}{R} + i\omega_1 C}, \quad V_2 = \frac{I_{c2} s_1 e^{i(\frac{\theta_0}{2} + \frac{\pi}{2})}}{\frac{1}{R} + i\omega_2 C}, \quad V_3 = \frac{I_{c1} e^{i(\theta_0 + \frac{\pi}{2})}}{\frac{1}{R} + i\omega_3 C}. \quad (49)$$

The AC equivalent circuit is that the DC current source is open circuit and the Josephson junction can be treated as the AC current source which applies to the parallel circuit contain resistor and capacitor. We can go further to the first order approximation by including the

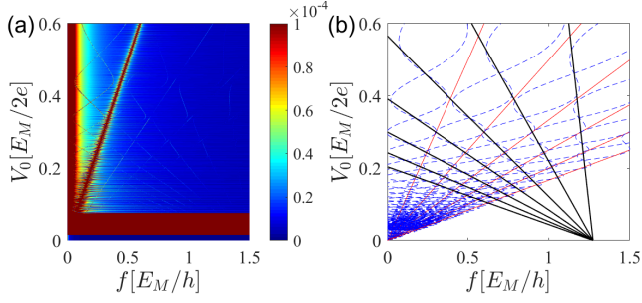


FIG. 4. (a) Numerical result of radiation spectrum when $\frac{\delta}{E_M}$ is large. Parameters are same as Fig.2 except $C = 0.2nF$ and $\frac{\delta}{E_M} = 0.35$; (b) Analytical results with the same parameters as (a). The function of black solid lines is Eq.(46).

Bessel function J_1 and taken $J_1(x) = x$ in Eqs. (33) and (36). Then we obtain,

$$\begin{aligned} j_0 &= l_0 = 1 \\ j_n &= A_n - iB_n = \frac{2e}{\hbar\omega_n} V_n^* \\ l_n &= \frac{e}{\hbar\omega_n} V_n^*. \end{aligned} \quad (50)$$

The first two equations of Eq. (47) now become

$$\begin{aligned} \left(\frac{1}{R} + i\omega_1 C\right) V_1 + i\frac{2eI_{c1}}{\hbar\omega_2} e^{i\theta_0} V_2 &= iI_{c2}s_1 e^{i\frac{\theta_0}{2}} \\ i\frac{2eI_{c1}}{\hbar\omega_1} e^{i\theta_0} V_1 + \left(\frac{1}{R} + i\omega_3 C\right) V_2 &= iI_{c2}s_1^* e^{i\frac{\theta_0}{2}}, \end{aligned} \quad (51)$$

with the solutions

$$V_1 = \frac{iI_{c2}s_1 e^{i\frac{\theta_0}{2}} \left(\frac{1}{R} + i\omega_2 C\right) + \frac{2eI_{c1}I_{c2}}{\hbar\omega_2} s_1^* e^{i\frac{3\theta_0}{2}}}{\left(\frac{1}{R} + i\omega_1 C\right) \left(\frac{1}{R} + i\omega_2 C\right) + \frac{4e^2 I_{c1}^2}{\hbar^2 \omega_1 \omega_2}} \quad (52)$$

$$V_2 = \frac{iI_{c2}s_1^* e^{i\frac{\theta_0}{2}} \left(\frac{1}{R} + i\omega_1 C\right) + \frac{2eI_{c1}I_{c2}}{\hbar\omega_1} s_1 e^{i\frac{3\theta_0}{2}}}{\left(\frac{1}{R} + i\omega_1 C\right) \left(\frac{1}{R} + i\omega_2 C\right) + \frac{4e^2 I_{c1}^2}{\hbar^2 \omega_1 \omega_2}} \quad (53)$$

$$V_3 = \frac{iI_{c1} e^{i\theta_0} + iI_{c2}s_1 \frac{e}{\hbar\omega_2} V_1^* e^{i\frac{\theta_0}{2}} + iI_{c2}s_1^* \frac{e}{\hbar\omega_1} V_2^* e^{i\frac{\theta_0}{2}}}{\frac{1}{R} + i\omega_3 C} \quad (54)$$

This gives the final analytical formula for the radiation intensity of the topological Josephson junction which includes the quantum dynamics of the two-level system formed by Majorana zero modes.

VII. $I - V$ CURVE OF JOSEPHSON JUNCTION

The direct current $I - V$ curve of Josephson junction can also be calculated by QRCSJ model²⁶. In the overdamping junction with large δ and $I_{c1} = 0$, due to the intrinsic Rabi oscillations of MZMs, even if there is no external AC excitation, the voltage steps will still appear in the $I - V$ curve when the input current I is

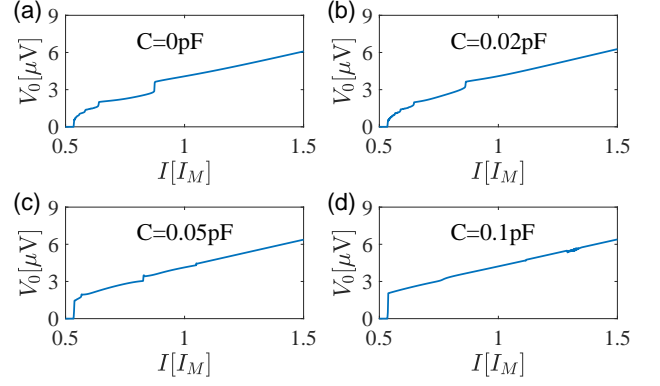


FIG. 5. The influence of capacitance on DC Shapiro steps. The capacitance of each junction is shown in the figure, with other parameters as same as Ref.³⁶.

small, which are described as DC Shapiro steps³⁶. We extend DC Shapiro steps to overdamped junctions, which is shown in Fig.5. It is clear that the junction capacitance has a significant effect on DC Shapiro steps. In the underdamped junction, the existence of capacitance weakens the Rabi oscillations of MZMs. Even if a small capacitance is applied, the DC Shapiro step will be suppressed, as shown in Fig.5.

VIII. CONCLUSION

In summary, we use quantum resistively shunted junction model to study the Josephson radiation. We obtain the radiation spectra with both numerical simulation and analytical approximation. For overdamped junction which has been explore experimentally, We find that emission lines corresponding to both 2π and 4π period Josephson effect^{12,21}. Unique to our model, we reveal that the 4π period emission line terminates at certain voltage due to the nonlinear quantum dynamics of the Majorana two-level system^{26,36}. As far as we known, our result provide the only theoretical explanation to the experiment observed feature¹⁷. For underdamped junction, we find that the 4π period Josephson emission presents oscillating patterns which are well described by a Bessel function. Further investigation shows that they are coming from the constructive Landau-Zener-Stückelberg interference of the Majorana two-level system. These patterns give a new feature for detecting the Majorana zero modes³⁷.

ACKNOWLEDGMENTS

This work was supported by NSFC (Nos.11774033 and 11974049) and Beijing Natural Science Foundation

(No. 1192011). We acknowledge the support of HSCC of Beijing Normal University, and some numerical

simulations in this work were performed on Tianhe in Beijing Computational Science Research Center.

-
- * wangzh356@mail.sysu.edu.cn
 † txma@bnu.edu.cn
- ¹ A. Kitaev, *Annals of Physics* **303**, 2 (2003).
 - ² J. Liu, L. Fu, B.-Y. Ou, S.-G. Chen, D.-I. Choi, B. Wu, and Q. Niu, *Phys. Rev. A* **66**, 023404 (2002).
 - ³ J. Alicea, *Reports on Progress in Physics* **75**, 076501 (2012).
 - ⁴ H.-J. Kwon, K. Sengupta, and V. M. Yakovenko, *The European Physical Journal B - Condensed Matter and Complex Systems* **37**, 349 (2004).
 - ⁵ L. P. Rokhinson, X. Liu, and J. K. Furdyna, *Nature Physics* **8**, 795 (2012).
 - ⁶ A. Y. Kitaev, *Physics-Uspekhi* **44**, 131 (2001).
 - ⁷ P. Matthews, P. Ribeiro, and A. M. García-García, *Phys. Rev. Lett.* **112**, 247001 (2014).
 - ⁸ B. Sothmann and E. M. Hankiewicz, *Phys. Rev. B* **94**, 081407 (2016).
 - ⁹ Y. Peng, Y. Vinkler-Aviv, P. W. Brouwer, L. I. Glazman, and F. von Oppen, *Phys. Rev. Lett.* **117**, 267001 (2016).
 - ¹⁰ H. Ren, F. Pientka, S. Hart, A. T. Pierce, M. Kosowsky, L. Lunczer, R. Schlereth, B. Scharf, E. M. Hankiewicz, L. W. Molenkamp, B. I. Halperin, and A. Yacoby, *Nature* **569**, 93 (2019).
 - ¹¹ A. Murani, B. Dassonneville, A. Kasumov, J. Basset, M. Ferrier, R. Deblock, S. Guéron, and H. Bouchiat, *Phys. Rev. Lett.* **122**, 076802 (2019).
 - ¹² F. Domínguez, O. Kashuba, E. Bocquillon, J. Wiedenmann, R. S. Deacon, T. M. Klapwijk, G. Platero, L. W. Molenkamp, B. Trauzettel, and E. M. Hankiewicz, *Phys. Rev. B* **95**, 195430 (2017).
 - ¹³ A. Stern and E. Berg, *Phys. Rev. Lett.* **122**, 107701 (2019).
 - ¹⁴ C. W. J. Beenakker, *Annual Review of Condensed Matter Physics* **4**, 113 (2013).
 - ¹⁵ M. Sato and Y. Ando, *Reports on Progress in Physics* **80**, 076501 (2017).
 - ¹⁶ H. Kamata, R. S. Deacon, S. Matsuo, K. Li, S. Jeppesen, L. Samuelson, H. Q. Xu, K. Ishibashi, and S. Tarucha, *Phys. Rev. B* **98**, 041302 (2018).
 - ¹⁷ R. S. Deacon, J. Wiedenmann, E. Bocquillon, F. Domínguez, T. M. Klapwijk, P. Leubner, C. Brüne, E. M. Hankiewicz, S. Tarucha, K. Ishibashi, H. Buhmann, and L. W. Molenkamp, *Phys. Rev. X* **7**, 021011 (2017).
 - ¹⁸ W.-C. Huang, Q.-F. Liang, D.-X. Yao, and Z. Wang, *Phys. Rev. A* **92**, 012308 (2015).
 - ¹⁹ C. Schrade and L. Fu, *Phys. Rev. Lett.* **120**, 267002 (2018).
 - ²⁰ D. Laroche, D. Bouman, D. J. van Woerkom, A. Proutski, C. Murthy, D. I. Pikulin, C. Nayak, R. J. J. van Gulik, J. Nygård, P. Krogstrup, L. P. Kouwenhoven, and A. Geresdi, *Nature Communications* **10**, 245 (2019).
 - ²¹ J. Wiedenmann, E. Bocquillon, R. S. Deacon, S. Hartinger, O. Herrmann, T. M. Klapwijk, L. Maier, C. Ames, C. Brüne, C. Gould, A. Oiwa, K. Ishibashi, S. Tarucha, H. Buhmann, and L. W. Molenkamp, *Nature Communications* **7**, 10303 (2016).
 - ²² P. San-Jose, E. Prada, and R. Aguado, *Phys. Rev. Lett.* **108**, 257001 (2012).
 - ²³ J. Picó-Cortés, F. Domínguez, and G. Platero, *Phys. Rev. B* **96**, 125438 (2017).
 - ²⁴ M. Houzet, J. S. Meyer, D. M. Badiane, and L. I. Glazman, *Phys. Rev. Lett.* **111**, 046401 (2013).
 - ²⁵ D. I. Pikulin and Y. V. Nazarov, *Phys. Rev. B* **86**, 140504 (2012).
 - ²⁶ J.-J. Feng, Z. Huang, Z. Wang, and Q. Niu, *Phys. Rev. B* **98**, 134515 (2018).
 - ²⁷ J.-J. Feng, Z. Huang, Z. Wang, and Q. Niu, *Phys. Rev. B* **101**, 180504 (2020).
 - ²⁸ Y. Tanaka, T. Yokoyama, and N. Nagaosa, *Phys. Rev. Lett.* **103**, 107002 (2009).
 - ²⁹ P. A. Ioselevich and M. V. Feigel'man, *Phys. Rev. Lett.* **106**, 077003 (2011).
 - ³⁰ J. B. Oostinga, L. Maier, P. Schüffelgen, D. Knott, C. Ames, C. Brüne, G. Tkachov, H. Buhmann, and L. W. Molenkamp, *Phys. Rev. X* **3**, 021007 (2013).
 - ³¹ L. Fu and C. L. Kane, *Phys. Rev. B* **79**, 161408 (2009).
 - ³² D. Sun and J. Liu, *Phys. Rev. B* **97**, 035311 (2018).
 - ³³ F. m. c. Crépin and B. Trauzettel, *Phys. Rev. Lett.* **112**, 077002 (2014).
 - ³⁴ F. Domínguez, F. Hassler, and G. Platero, *Phys. Rev. B* **86**, 140503 (2012).
 - ³⁵ J. Cayao, P. San-Jose, A. M. Black-Schaffer, R. Aguado, and E. Prada, *Phys. Rev. B* **96**, 205425 (2017).
 - ³⁶ S.-J. Choi, A. Calzona, and B. Trauzettel, *Phys. Rev. B* **102**, 140501 (2020).
 - ³⁷ S. Shevchenko, S. Ashhab, and F. Nori, *Physics Reports* **492**, 1 (2010).